AIAA AVIATION Forum
8-12 June 2026, San Diego, CA
AIAA AVIATION 2026 Forum

10.2514/6.2026-4729

Power optimization strategies for a converter-free multi-stack fuel cell system in near MW-range

K. Sommer[1], T. Braun[2] and C. Bänsch[3]
German Aerospace Center (DLR), Stuttgart, Baden-Württemberg, 70197, Germany

I. Nomenclature

2s4p	=	2-series & 4-parallel multi-stack fuel cell system
CL	=	Catalyst layer
CP	=	Check point
CV	=	Cell voltage
DLR	=	Deutsches Zentrum für Luft- und Raumfahrt e.V. - German Aerospace Center
ES	=	E-Storage - regenerative 2-quadrant DC source/sink
JRC	=	European Commission's Joint Research Centre
MFCS	=	Multi-stack fuel cell system
MW	=	Megawatt
OCV	=	Open-circuit voltage
PDU	=	Power distribution unit
PEMFC	=	Polymer electrolyte membrane fuel cell
UUT	=	Units under test

II. Abstract

Hydrogen-electric propulsion based on polymer electrolyte membrane fuel cells is considered a promising technology for zero-emission powertrains in small and regional aircraft. Achieving megawatt-class power levels requires multi-stack fuel cell systems, in which several fuel cell modules are electrically interconnected. In converter-free architectures, electrical interactions between stacks can significantly influence the achievable system performance. This study experimentally investigates power optimization strategies for a near-megawatt multi-stack fuel cell system at the BALIS test facility of the German Aerospace Center. The investigated system consists of eight identical polymer electrolyte membrane fuel cell modules (~100 kW each) arranged in a 2-series/4-parallel configuration with master-slave control within each series pair.

Two approaches to enhance overall system power are examined. First, module pairing is optimized based on experimentally determined polarization characteristics to minimize voltage deviations between parallel strings. Reconfiguration of the modules reduces current imbalance and increases the maximum system current from 1450 A to 1560 A, resulting in a 7 % increase in peak power from 790 kW to 848 kW. Second, the influence of reversible stack degradation on system performance is analyzed using standardized polarization curve measurements and four adapted recovery procedures. Voltage Pulsing was the only recovery procedure, which led to a performance increase of around 0.4 %. The low impact of the recovery procedures is assumed to result from facility constraints, fuel cell controller interventions, and low reversible degradation of the fuel cells. Nevertheless, the proposed procedures can serve as an indication of how a targeted reduction of reversible degradation can be achieved in future aviation systems and thus improve the performance of converter-free architectures in application-relevant long-term operation.

Future studies should focus on degraded operation to demonstrate the potential of the recovery procedures and the comparison of fuel cell system architecture variants, also considering the integration of DCDC converters.

[1] Researcher, German Aerospace Center (DLR), Institute of Engineering Thermodynamics
[2] Master student, German Aerospace Center (DLR), Institute of Engineering Thermodynamics
[3] Group leader, German Aerospace Center (DLR), Institute of Engineering Thermodynamics

III. Introduction

Among several emerging approaches towards sustainable propulsion technologies, hydrogen-electric propulsion has gained significant attention as a promising solution for small and regional aircraft [1–3]. Polymer electrolyte membrane fuel cells (PEMFCs) represent a viable technology for converting hydrogen into electrical power with high efficiency and zero local emissions [4,5]. To achieve megawatt-class propulsion capability, fuel cell systems must be appropriately scaled, which can be accomplished by implementing multi-stack fuel cell systems (MFCS) consisting of multiple fuel cell stacks arranged in series and/or parallel configurations [6,7]. Such architectures offer enhanced flexibility with respect to fault tolerance and system scalability. The development of optimized topologies, including DC/DC-converter-free configurations, provides opportunities to reduce system complexity and overall weight while maintaining sufficient energy supply for future electric propulsion applications. Demonstrators developed by companies such as Airbus[4], Universal Hydrogen[5] and Beyond Aero[6] highlight the technical feasibility of megawatt-class hydrogen-electric propulsion; however, comprehensive scientific evaluations of these systems remain limited. After having achieved the megawatt prove of performance[7] and a first characterization of the BALIS fuel cell system of the German Aerospace Center (DLR) in previous studies [8,9], in this work a targeted reorganization of the fuel cell modules to increase system power in the existing MFCS is examined and recovery procedures to reduce reversible degradation in application-relevant systems are investigated. All experiments in this work have been performed between August 2025 and April 2026.

IV. Experimental setup & procedure

A. Test facility setup

The BALIS[8] research facility at the DLR was established to systematically investigate the performance, operational behavior, and interaction mechanisms of MFCS under aviation-relevant conditions [10,11]. The overall BALIS test environment follows a modular approach with test fields for the different powertrain subsystems liquid hydrogen tank, fuel cell system, power electronics, e-drive and battery system. In the test fields the subsystems can be investigated separately or connected via the infrastructure. In the present study, a near-megawatt MFCS is experimentally optimized within this facility. Focus is placed on the electrical interactions and coupling effects within this converter-free architecture. Hence, only a brief description of the electrical part of the system is given here. The MFCS, which is illustrated in Figure 1, consists of eight individual PEMFC modules (built by PowerCell, PS-100, $P_{Gross} = 120\ \text{kW}, 420\ \text{A}$) configured in a 2-series, 4-parallel (2s4p) arrangement, each providing approximately 100 kW of net power. Additional modules are available as back-up modules in separate test places, which are not active in this study. Within each pair of series-connected modules, a master-slave control structure is implemented, while the four pairs operate at a common voltage level in a parallel configuration. The maximum current output of each pair is limited to 400 A due to built-in fuses in the two power distribution units (PDU) on the facility site. On the other hand, the minimum used current is set to at least 50 A per system, as the used module controller ensures that operation is not possible close to the open circuit voltage (OCV). If the current drops below 40 A for longer than 30 s, the controller initiates a controlled soft shutdown to protect the stack from degradation. Each bus bar is interfaced with a regenerative two-quadrant DC source/sink, referred to as E-Storage (ES), providing a power capacity of 825 kW (built by AVL, 1250 A / 1200 V) per unit. Two of these loads are operated jointly as a single combined load. Diodes installed in the PDU prevent any positive current flow, thereby protecting the fuel cell systems. High-voltage (0–500 V, rated 500 V) and low-voltage (0–60 V, rated 24 V) auxiliary power are supplied by the facility infrastructure and must be considered when balancing the chemical process. Two auxiliary units are connected in series and supply a pair of

[4] Airbus press release available from (visited at 2025.10.21):
https://www.airbus.com/en/newsroom/stories/2024-01-first-zeroe-engine-fuel-cell-successfully-powers-on
[5] Universal Hydrogen press release available from (visited at 2025.10.20):
https://fuelcellsworks.com/news/universal-hydrogen-completes-first-full-demonstration-of-ampcart-h2
[6] Beyond Aero press release available from (visited at 2025.10.20):
https://www.aerospacetestinginternational.com/news/beyond-aero-hits-key-testing-milestone-with-hydrogen-electric-aircraft-propulsion-system.html
[7] DLR press release available from (visited at 20.04.2026):
https://www.dlr.de/en/latest/news/2025/balis-test-system-components-cross-megawatt-threshold-for-the-first-time
[8] More information available online about BALIS a Fuel cell-based powertrain for aircraft 1.5+ MW (visited at 2025.10.20): https://www.dlr.de/de/tt/forschung-transfer/forschungsinfrastruktur/testeinrichtungen/balis

modules via a string connection box. Due to spatial constraints, the auxiliary supply units are located in a separate container adjacent to the fuel cell system. This study focuses on electrical interactions and coupling effects within the converter-free architecture, which are critical for stability, efficiency, and performance at near-megawatt power levels. Thermal management, gas infrastructure, and measurement systems are beyond the scope of this work. Further Information about the test facility can be found in [8–11].

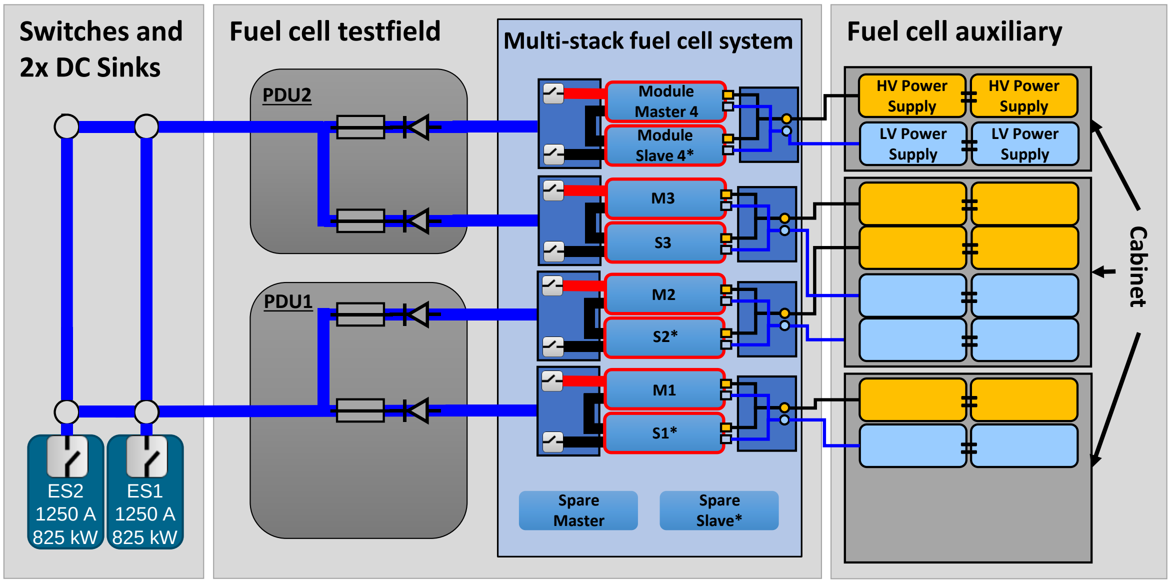

Figure 1 Electrical architecture of the applied fuel cell system. Thick blue lines indicate the active power lines of the high voltage system. Module Master 1-4 paired each with Module Slaves 1-4. Red framed system names are active during this work, two spares present.

B. Performance increases through recombination of modules

In the first part of this study, the maximum power output capability of the MFCS is extended through an advantageous combination of the master and slave modules. For this purpose, the *U*/*I* characteristics of the individual modules are determined. Based on the single module performance, the master slave pairs are combined in such a way that the deviation of the resulting string voltages at maximum string current of 400 A is minimized. This method involves the physical reconfiguration of available modules on site. Due to differing integrated connector configurations, master modules cannot be substituted for slave modules and vice versa. With this approach it can be avoided that the most powerful string has already reached its current limit, while the other strings can only supply a relatively low current at the necessarily uniform bus voltage, limiting the achievable maximum system power compared to the sum of the individual string power values. While it is possible to set the optimization target point to any voltage level, in this study the maximum power point is chosen as reference. In order to establish a standardized approach for stack characterization, polarization curves of the different strings are measured separately before and after recombination based on the protocol of the European Commission’s Joint Research Centre (JRC) fulfilling pre-defined steady-state criteria [12]. In addition, the performance change of the full system in parallel operation which is achieved by the module recombination is investigated by a test procedure based on stationary measuring points at different load levels of 400 A, 600 A, 800 A, 1200 A and 1400 A. The final stage above the 1400 A level is tested manually with incremental increases of 10 A up to a distribution which can be held for at least 10 min while respecting the fuse limit of 400 A at string level.

C. Performance increases through recovery procedures

With the fuel cell system obtained after recombination, an extensive test campaign was carried out. All eight modules in questions experienced around 70 hours of operation with around 16 hours being between 80 % and 100 % of their individual power limit and around 50 start-ups. During this testing period, the UUTs experienced different test blocks including current ramp profiles from idle to maximum power, application-relevant load cycles incl. highly dynamic load profiles, and failure injection tests which will not be discussed in detail. Meaning two modules per string have experienced identical operating histories, including comparable shutdown events, load hours, and operating points, were subjected to the same regeneration method. Within this work, the influence of reversible stack degradation on the overall system performance after the test campaign is analyzed. Recovery measures from the literature, originally developed under laboratory conditions, are adopted for the application in commercial MFCS and scaled to relevant power levels. Due to operational and hardware constraints of the facility and fuel cell modules the proposed procedures, adapted regeneration procedures were derived taking the restrictions into account. Each procedure was carried out starting from a prewarmed state of the systems. To reach that state, the systems were running for 12,5 min at 100 A each per string. To characterize the system state polarization curves before and after the test campaign and the application of recovery procedures were recorded. In total, four different recovery methods were applied to four different module pairs: M1S1 - Voltage pulsing, M2S2 - Voltage Sweeping, M3M3 - full power in presence of liquid water, M4S4 - JRC. In the following sections the applied recovery procedures are described in detail.

Voltage pulsing. The objective of voltage pulsing is to mitigate performance degradation caused by catalyst surface contamination. The application of dynamic voltage profiles enables access to multiple potential regimes, allowing simultaneous treatment of different contamination mechanisms. At high cathode potentials contaminants like Sulfur and NOx are oxidized to sulfate and nitrate, which will then be able to be desorbed at low cathode potentials together with other contaminants like CO_2 from CO-poisoning and OH- from reduced PtOx [13–15]. The detailed order of one pulse sequence is described in Table 1. As the used modules have two different ramp-up limits for specific current areas, step number 4 is divided. The first part 4.1 includes a 10 A/s ramp between $I_{\mathrm{Start}} = 10\ A$ and $I_{\mathrm{End}} = 45\ A$ to accommodate for slower starting reactions when leaving OCV, the second part 4.2 includes a 50 A/s ramp to the desired maximum current point. The voltage pulsing method is carried out 5-7 times per loop passage to have a relevant resulting in a total procedure duration about 1 hour.

Table 1 Voltage pulsing sequence of a single pulse

	Step	I_{start} [A]	I_{end} [A]	Ramp [A/s]	Duration [s]	Possible recovery mechanisms	Literature used
1	→ Prewarmed-state	100	100	0	30	-	
2	↓ Current decrease	100	0	-100	1	-	
3	→ Holding time OCV	0	0	0	23.5	High cathode potential removing S- and NOx- cat.CL	[13,14]
4.1	↑ Current increase	0	45	10	4.5	-	
4.2	↑ Current increase	45	410	50	7.3	-	
5	→ Holding time at max. current	410	410	0	120	PtOx reduction, recovery of CO-poisoning and removal of sulfate anions by low cathode potential	[13,14,16]
6	↓ Current decrease	410	100	-100	3.1	-	
7	→ Prewarmed-state	100	100	0	30	--	
The total length of a single pulse cycle sums up to approximately 3 ½ min							

Voltage sweeping. With this procedure the goal is to recreate the voltage curve of a potential driven sweep. Cell voltages down to 0.2 V can lead to recovery of kinetic losses due to reduction of PtOx [13] and re-attachment of detached platinum nanoparticles onto the carbon support material [17]. Furthermore, recovery of mass transport losses is provided by the removal of hydrophilic oxide groups on the carbon surface caused by carbon corrosion [17]. Voltage is also known to remove other contaminants from the catalyst surface [18]. As current driven operation alone will not reach a cell voltage (CV) lower than ~0.55 V with the UUTs, for this procedure lean air operation [19] is adapted. In the reference study lean air operation originally initiated during operating phases within a current density range of 0.037 A/cm² to 0.089 A/cm² in order to mitigate Pt oxidation and perform regenerative voltage sweeps instead. These values correspond here to oxygen starvation at 40 A. When the condition of step 3.2 in Table 3 is met, the current is lowered to 15 A (=0.05 A/cm²). Low cell voltage decay rates defined in this study were applied, with target values of 0.4 V (mean) and 0.3 V (minimum). These values were selected based on the requirement that the reduction of PtOx on the cathode surface occurs at potentials below 0.4 V [20]. Operation below 40 A is subject to strict time constraints imposed by the fuel cell controller, which limits such conditions to durations shorter than 30 s. Therefore the point will be named t-boundary. To avoid harmful operating conditions such as cell reversal or hotspots resulting from air starvation [21], a series of limiting conditions are set for when the protocol is active. Within the aforementioned current density range, the stoichiometric air ratio is lowered, resulting in a cell voltage decay where fuel distribution is insufficient. Oxygen starvation was achieved by significantly reducing the air supply via the facility-side air flap while simultaneously introducing external nitrogen. If the blockade of cathode air isn't sufficient enough, the applied current can be gradually increased to 100 A. The voltage sweeping method is carried out 5-7 times per loop passage resulting in a total procedure duration about 1 hour.

Table 2 Voltage sweeping - Sequence of a single sweep

	Step	I_{start} [A]	I_{end} [A]	Ramp [A/s]	Duration	Termination condition	Literature used
1	Prewarmed-state	100	100	0	-	Preparations finished	-
2	↓ t-boundary	100	40	-60	1 s	-	-
3.1	→ Ox-starv.						[19,22]
3.2	t-boundary	40	40	0	-	CV_{mean} < 0.4 V or CV_{min} < 0.3 V	[19,23]
4	↓ I_{min}	40	15	-25	1 s	-	[19,21]
5	I_{min}	15	15	0	27 s	CV_{min} < 0.2 V	[19]
6.1	╳ Ox-starv.						
6.2	↑ t-boundary	15	40	25	1 s	-	
7	t-boundary	40	40	0	-	CV normalized	
8	↑ Idle	40	100	30	2 s	-	

Full power in presence of liquid water. The second regeneration approach is based on refs. [13–15] using the combined influence of high current density operation and the presence of liquid water. The procedure is described in Table 1. As the PS100 modules are equipped with an internal bypass in the high-temperature cooling circuit and a controller that maintains a constant inlet temperature of 68 °C, continuous adjustment of the operating temperature during operation is not feasible. Instead, temperature drops were induced to the stack by rapidly decreasing the cooling water temperature, thereby inducing condensation before the internal control system could compensate. This strategy was realized via the control of the facility cooling system, where the temperature set point $T_{\mathrm{HT,Set}}$ of the module inlet temperature can be varied between 20 and 65 °C. The full power in presence of liquid water method is carried out 5-7 times per loop passage resulting in a total procedure duration about 1 hour. In contrast to all other procedures applied in this work, this method can be used during operation. Recovery time is introduced to allow the system to stabilize when the voltage deviation between the lowest-performing cell and the stack average exceeds 100 mV because the because in this case the current is limited by the module-internal controller to 100 A until the cell voltage difference is below the limit again.

Table 3 Full power in presence of liquid water –
Sequence of a single temperature shock based on [13–15]

	Step	$T_{\mathrm{HT,Set,Start}}$ [°C]	$T_{\mathrm{HT,Set,End}}$ [°C]	Details
0	Preparation	-	-	Lower temperature of BALIS cooling circuit
1	Warmup	60	65	Increase temperature slowly to open bypass valve without derating of modules
2	Stabilization	65		Wait for stabilization of system and maximum bypass valve opening
3	Temperature drop	65	20	Quickest possible drop of $T_{\mathrm{HT,Set}}$ to maximize stack cooling before valve reacts
4	Cooldown	20		Hold until $T_{\mathrm{HT,Out}}$ reached low point due to valve closing
5	Warmup	20	60	Start warmup with high $\Delta T_{\mathrm{HT,Set}}$ to mitigate further valve closing and resulting waiting time, continue with low $\Delta T_{\mathrm{HT,Set}}$ to evade derating

JRC. The JRC recovery protocol was selected due to its established use as a reference in literature. It consists of five steps, which are described in Table 4. The protocol is based on ref. [24] and adaptions from ref. [25] with further adaptations due to system constraints. These changes can be summarized as follows: N_2 supply limitations required sequential purging of cathode and anode. To prevent membrane dry-out the N_2 purge duration set to 10 min. The modules are preheated prior to shutdown to promote water condensation during the rest phase. Artificial air gas cylinders (20 % O_2, 80 % N_2, 50 l at 200 bar) are used for anode air purge. The adaptions to the original JRC in sequential purging of cathode/anode and reducing the time to 10 minutes are marked in the table with “*”. The JRC method was planned to carried out once.

Table 4 JRC recovery protocol

	Step	Cathode	Anode	Duration	Possible recovery mechanisms	Literature used
1	H_2 soak	Shut off	H_2	Until CV = 0 + 10 min	PtOx reduction and removal of sulfate anions by low cathode potential	[22,24,26,27]
2	N_2 purge	N_2*		10 min*	Remove H2 (for safety reasons) and excess water	[25,27,28]
3	Air purge	Air *		30 min	Remove CO and other contaminants from the anodic surface by increased anode potential	[28–30]
4	Shutdown	Stop gas supply; release pressure; open cell outlets		~8 h (overnight)	PtOx reduction and removal of sulfate anions by low cathode potential; regeneration/hydration by condensed product water	[18,22,28,31–35]
5	N_2 purge	N_2*		10 min*	Remove water to avoid flooding	[36,37]

Loop-Scheme. A checkpoint-based logic based on ref. [17] is integrated into the active testing loop for the recovery procedures “full power in presence of liquid water”, “voltage pulsing” and “voltage sweeping”, which is illustrated in Figure 2. Within this checkpoint scheme, holding periods of 5 minutes at full-load of 400 A and a part-load of 100 A are used for evaluation during regeneration. At least two cycles of regeneration are carried out to avoid interruptions due to statistical effects.

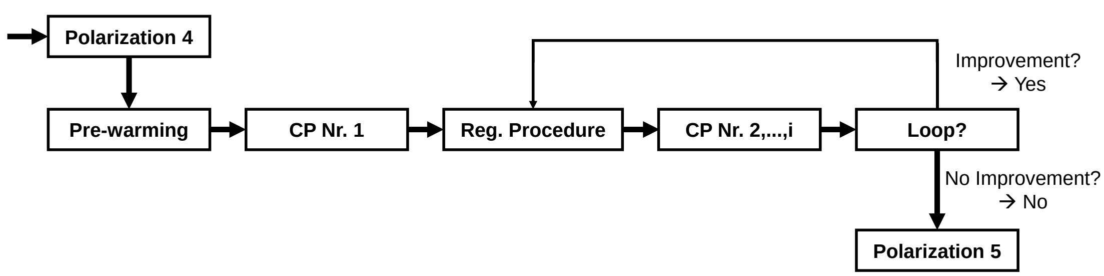

Figure 2 Voltage checkpoint (CP) loop-scheme

V.Results and discussion

A. Results of the recombination

The modules were reconfigured by pairing the master module with the highest voltage at 400 A with the slave module exhibiting the lowest voltage value, the second-highest master with the second-lowest slave, and so forth. One additional string with two modules serving as spare modules was also considered for recombination. This pairing strategy yielded the narrowest distribution of string voltages and the minimum achievable standard deviation among the available units. Alternative combination strategies were also evaluated but resulted in a wider spread in string voltage levels at the designated design point. The recombination data is shown in Table 5. The maximum string voltage difference could be reduced from 22 V (4 %) before recombination to 4 V (1 %) after recombination. To give an optic indication of that change, in Figure 1 the affected modules are marked with (*) after their module number.

Table 5 Test Recombination to optimize string voltage at 400 A per module with their individual stack voltages – experimental data

String Number	Module Number	Stack Voltage before, V	String Voltage before, V	Recombination	String Voltage after, V
1	M1	265	546	-	541
	S1	281		→ New S2	
2	M2	260	537	-	540
	S2	277		→ New S1	
3	M3	275	543	-	543
	S3	268		-	
4	M4	259	524	-	544
	S4	265		→ New S(spare)	
spare	M(spare)	288	573	-	553
	S(spare)	285		→ New S4	
Max. Voltage difference[9]			22		4

The measured polarization curves of the different strings before and after recombination is shown in Figure 3. The results show that the reduction of voltage differences between the different strings is only valid for the targeted load point at 400 A. At lower currents the differences stayed the same or even increased.

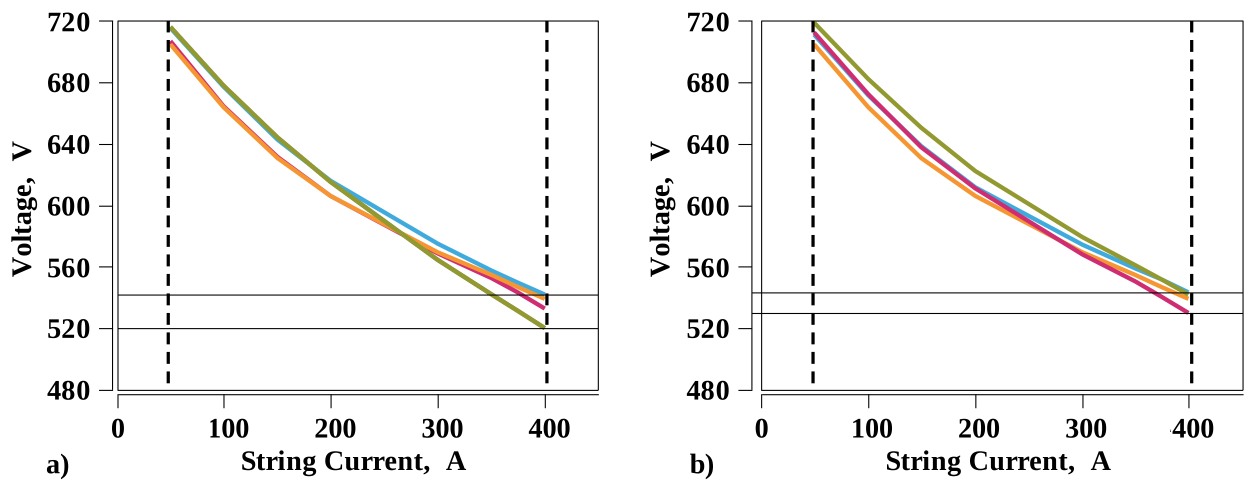

Figure 3 Polarization curves of the different strings a) before recombination and b) after recombination. Blue M1S1, red M2S2, yellow M3M3, green M4S4. Black horizontal lines indicate the difference in maximum and minimum string voltage at a current of 400A.

[9] Difference between the highest and lowest voltage between the four active strings.

The string current outputs during parallel operation at maximum power before and after recombination of the modules is illustrated in Figure 4. In this comparison run the overall current was permanently increased in small steps to seek out the maximum system current when the best-performing string has reached the 400 A facility limit. A substantial reduction of the string current deviation at the target load point was achieved with all pairs operating close to their string current limit. As a result, the overall maximum current could be increased by 8 % from 1450 A to 1560 A and the maximum system power by 7 % from 790 kW to 848 kW. Note that inserting the Spare Slave module into the active testing pool contributed to an improvement of 8 kW at 400 A, just because of its higher achievable maximum power compared to the module applied before recombination (at 400 A: new 114 kW vs old 106 kW).

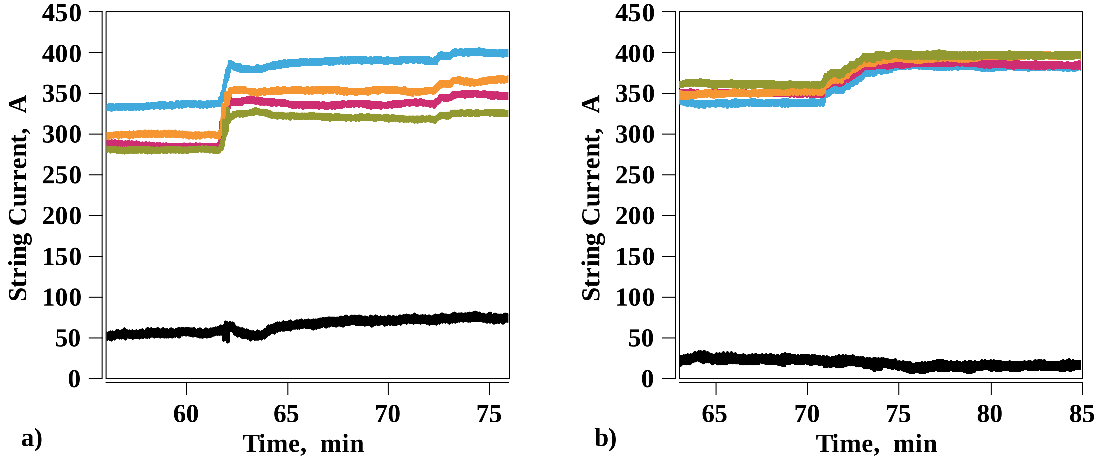

Figure 4 String currents over time during full parallel system operation at respective maximum load a) before optimization with total system current: 1450 A), b) after optimization with total system current: 1560 A); Colored lines: current per active string #1-4; Black line: maximum deviation of the string currents.

B. Results of the recovery procedures

The test results of the recovery procedure "Voltage Pulsing" are taken as an example for the discussion. A detailed discussion of the recorded test data of all recovery procedures is beyond the scope of this work. In Figure 5 the measured average cell voltage and the string current is shown during the first group of five pulses between 35 min and 55 min, followed by the second checkpoint between 55 min and 77 min. Afterwards the start of the second group of pulses is visible. The average voltage of the master stack exhibits both higher peaks and lower minima, indicating a more pronounced dynamic response and an overall stronger reaction to the applied regeneration procedure than the slave module.

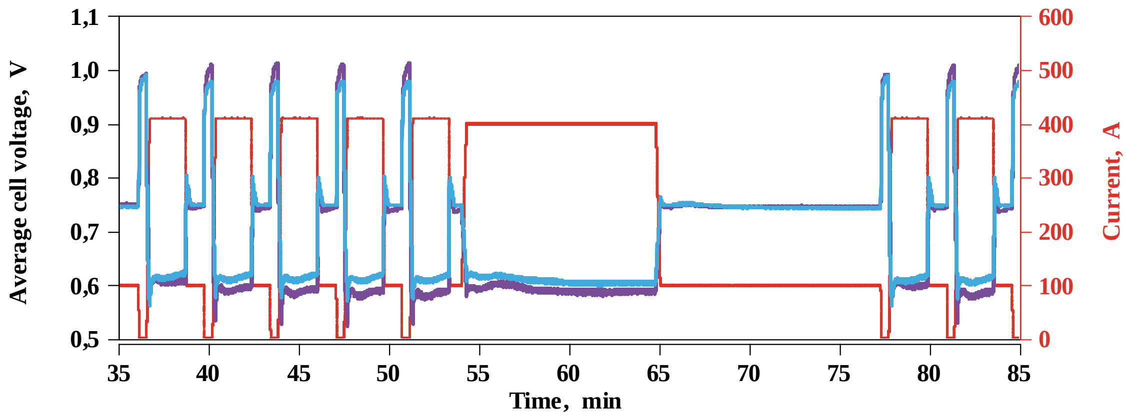

Figure 5 Test data during the recovery procedure *Voltage Pulsing* during a time period of 50 min starting with the first set of voltage pulses; Purple: average cell voltage of master module; Blue: average cell voltage of slave module.

In Table 6 the evolution of voltage checkpoints is summarized. For all procedures a reduction of voltage at both, the 100 A and 400 A checkpoints, were observed over the course of their execution. Hence, in no cases an improvement was recorded and therefore each procedure was stopped after the second loop.

Table 6 Voltage Checkpoints - Comparison

	Full power in presence of liquid water		Voltage Pulsing		Voltage Sweep	
	U_{100A}	U_{400A}	U_{100A}	U_{400A}	U_{100A}	U_{400A}
CP 1 [V]	676.8	552.8	679.7	548.8	676.7	524.5
$\Delta_{1\rightarrow2}$	-0.5 %	-3.1 %	-0.4 %	-1.6 %	-0.1 %	-0.7 %
CP 2 [V]	673.3	535.6	676.9	540.3	676.3	520.9
$\Delta_{2\rightarrow3}$	-0.50 %	-1.7 %	-0.2 %	-0.7 %	-0.4 %	-2.9 %
CP 3 [V]	669.9	526.6	675.4	536.6	673.5	505.5

The measured polarization curves before and after the conduction of the recovery procedures are shown in Figure 6. The results confirm the observations during the conduction of the procedures at the checkpoints for most cases. The highest deviation is observed for the “Full power with liquid water” procedure, where a reduction of the voltage of 3,3 % is obtained after the recovery procedure. A small improvement of the system performance is observed for the “Voltage pulsing”. The voltage at 400 A increased by 0.4 %. However, it is assumed that this number is below the statistical uncertainty of the measurement. Altogether, no performance improvements of the present fuel cell system could be achieved with the recovery procedures.

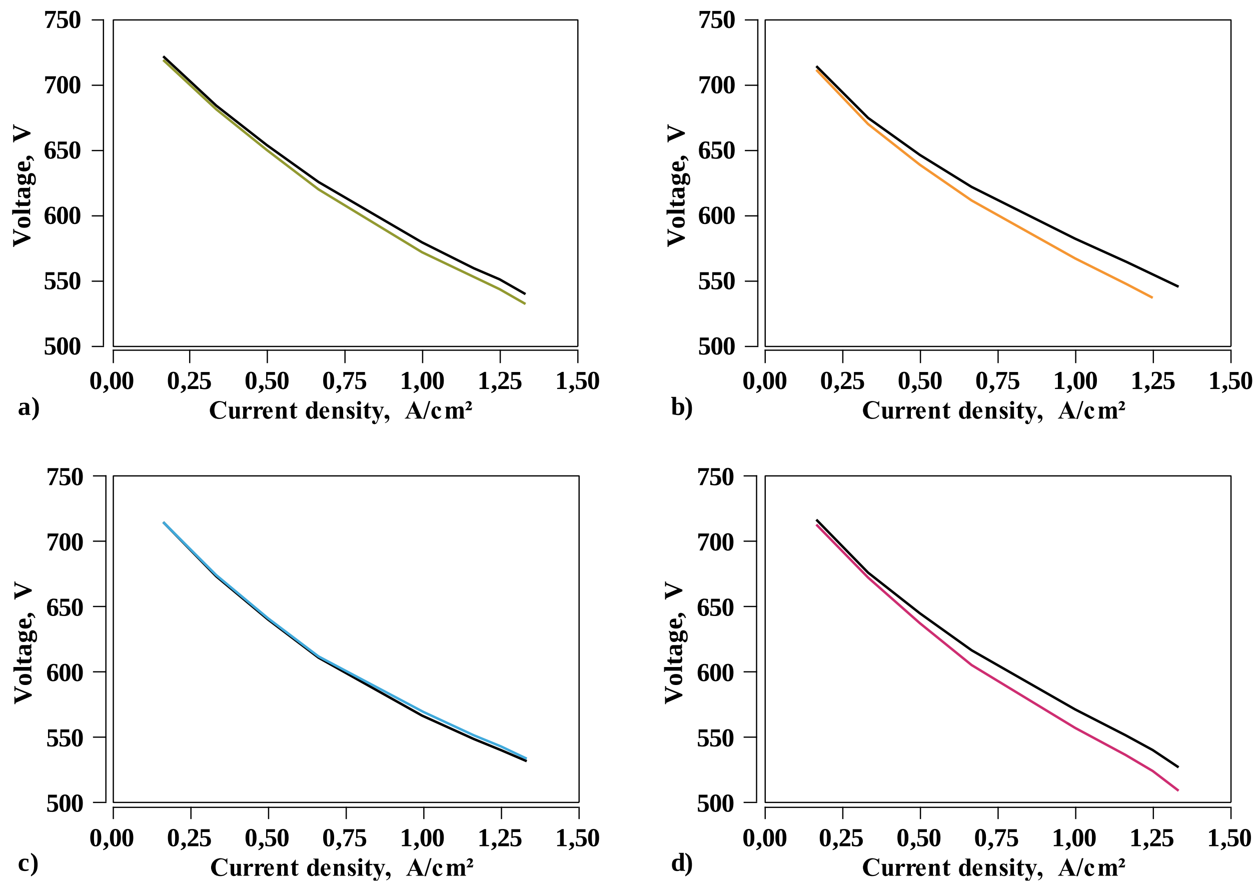

Figure 6 Comparison in polarization values before (black) and after (colored) the applied regeneration methods. a) JRC b) Full power with liquid water c) Voltage Pulsing d) Voltage sweeping

An extensive interpretation of the test data is difficult due to the low number of test data. However, it can be assumed that the reversible degradation in the system is low given the still low number of operating hours and demanding operating conditions, so that the various regeneration cycles cannot have any effect. Therefore, at this stage, it is not yet possible to draw any conclusions regarding the effectiveness and suitability of the various methods.

VI. Conclusion

Overall, the results demonstrate that power optimization in the parallel operation of a converter-free MFCS is achievable and enables harmonization of operating characteristics at specific load points. Reconfiguration of modules based on their individual voltage behavior provides significant improvements without further adjustments or efficiency losses and can be targeted for a specific area of interest. As already low voltage differences between strings or modules in direct parallel architectures can have significant impact on the system performance, this method has potential for power improvements with low effort.

Furthermore, applying targeted recovery strategies for reversible degradation in individual modules can further enhance overall MFCS performance, but they can also generate additional short-term disturbance on stack level. Nevertheless, it is shown that regeneration procedures developed on a laboratory scale can be transferred to application-relevant high-performance systems, even if adaptations and simplifications are necessary in some cases due to the technical limitations at system level. Combining the observations of the recombination and regeneration test is can be assumed that targeted regeneration of degraded stacks with the goal to harmonize deviating voltage levels in parallel converter-free multi-stack configurations is possible. Furthermore, it can constitute a measure also in application-relevant maintenance procedures to improve not only the performance of the regenerated stack but also specifically the system performance without disassembling the full system or exchange of modules. Operational target should be to keep the string current deviation at a fixed voltage level in parallel operation as low as possible.

In future studies the suitability of the proposed procedures should be tested on degraded systems and the integrability in application-relevant maintenance processes should be investigated. The potential of targeted regeneration to harmonize the voltage levels in parallel converter-free configurations should be compared to procedures in which all stacks of the system are regenerated as good as possible. Furthermore, the integration of DCDC-converters to enable a separate control of the voltage levels of the different strings should be considered and compared to the converter-free architecture.

Acknowledgement

CLEAN AVIATION

Funding: The project is supported by the Clean Aviation Joint Undertaking and its members in the framework of Grant Agreement n° 101102020 – AMBER.

Co-funded by the European Union

Funded by the European Union. Views and opinions expressed are however those of the author(s) only and do not necessarily reflect those of the European Union or Clean Aviation Joint Undertaking. Neither the European Union nor the granting authority can be held responsible for them.

References

[1] Baroutaji, A., Wilberforce, T., Ramadan, M., and Olabi, A. G., "Comprehensive Investigation on Hydrogen and Fuel Cell Technology in the Aviation and Aerospace Sectors," *Renewable and Sustainable Energy Reviews*, Vol. 106, 2019, pp. 31–40. https://doi.org/10.1016/j.rser.2019.02.022

[2] Dahal, K., Brynolf, S., Xisto, C., Hansson, J., Grahn, M., Grönstedt, T., and Lehtveer, M., “Techno-Economic Review of Alternative Fuels and Propulsion Systems for the Aviation Sector,” *Renewable and Sustainable Energy Reviews*, Vol. 151, 2021, p. 111564. https://doi.org/10.1016/j.rser.2021.111564

[3] I. Dincer, C. A., “A Review on Potential Use of Hydrogen in Aviation Applications,” *Int. J. Sustain. Aviat.*, Vol. 2, 2016, pp. 74–100. https://doi.org/10.1504/IJSA.2016.076077

[4] Kazula, S., Staggat, M., and Graaf, S. D., “Functional and Safety Challenges of Hydrogen Fuel Cell Systems for Application in Electrified Regional Aircraft,” *Journal of Physics: Conference Series*, Vol. 2526, No. 1, 2023, p. 012063. https://doi.org/10.1088/1742-6596/2526/1/012063

[5] Baroutaji, A., Wilberforce, T., Ramadan, M., and Olabi, A. G., “Comprehensive Investigation on Hydrogen and Fuel Cell Technology in the Aviation and Aerospace Sectors,” *Renewable and Sustainable Energy Reviews*, Vol. 106, 2019, pp. 31–40. https://doi.org/10.1016/j.rser.2019.02.022

[6] Zhou, S., Fan, L., Zhang, G., Gao, J., Lu, Y., Zhao, P., Wen, C., Shi, L., and Hu, Z., “A Review on Proton Exchange Membrane Multi-Stack Fuel Cell Systems: Architecture, Performance, and Power Management,” *Applied Energy*, Vol. 310, 2022, p. 118555. https://doi.org/10.1016/j.apenergy.2022.118555

[7] Qiu, Y., Zeng, T., Zhang, C., Wang, G., Wang, Y., Hu, Z., Meng Yan, and Wei, Z., “Progress and Challenges in Multi-Stack Fuel Cell System for High Power Applications: Architecture and Energy Management,” *Green Energy and Intelligent Transportation*, Vol. 2, No. 2, 2023, p. 100068. https://doi.org/10.1016/j.geits.2023.100068

[8] Bänsch, C., Sommer, K., Weiss, J., and Gienger, A., “Experimental Investigation of the Efficiency of a MultiStack Fuel Cell System for Aviation Applications in the Megawatt Range,” *EUCASS*, 2025, p. 12 pages. https://doi.org/10.13009/EUCASS2025-399

[9] Sommer, K., Ni, B., Weiss, J., Thalau, O., and Bänsch, C., “Performance Analysis of a Megawatt Fuel Cell-Based Electric Powertrain for Regional Aircraft,” *EUCASS*, 2025, p. 10 pages. https://doi.org/10.13009/EUCASS2025-202

[10] Fritz, J., “Systems Engineering Methodology on a Multi-Integration Test Environment for Fuel Cell Flight Propulsion Systems.”

[11] Weiss, J., Diarra, D., Sommer, K., Ni, B., Thalau, O., and Bänsch, C., “Modular Test Environment for Fuel Cell-Based Electric Powertrains for Aviation: Methodological Approach of the Balis Test Fields Fuel Cell, Battery and E-Drive,” 2025, p. 6 pages. https://doi.org/10.25967/630212

[12] Tsotridis, G., Pilenga, A., De Marco, G., and Malkow, T., “EU Harmonised Test Protocols for PEMFC MEA Testing in Single Cell Configuration for Automotive Applications,” Publications Office of the European Union, Luxembourg, 2015. https://doi.org/10.2790/54653

[13] Mitzel, J., Zhang, Q., Gazdzicki, P., and Friedrich, K. A., “Review on Mechanisms and Recovery Procedures for Reversible Performance Losses in Polymer Electrolyte Membrane Fuel Cells,” *Journal of Power Sources*, Vol. 488, 2021, p. 229375. https://doi.org/10.1016/j.jpowsour.2020.229375

[14] Urdampilleta, I., Uribe, F., Rockward, T., Brosha, E. L., Pivovar, B., and Garzon, F. H., “PEMFC Poisoning with H2S: Dependence on Operating Conditions,” *ECS Transactions*, Vol. 11, No. 1, 2007, pp. 831–842. https://doi.org/10.1149/1.2780996

[15] Uribe, F. A., Springer, T. E., and Gottesfeld, S., “A Microelectrode Study of Oxygen Reduction at the Platinum/Recast-Nafion Film Interface,” *Journal of The Electrochemical Society*, Vol. 139, No. 3, 1992, pp. 765–773. https://doi.org/10.1149/1.2069299

[16] Uribe, F. A., and Zawodzinski, T. A., “A Study of Polymer Electrolyte Fuel Cell Performance at High Voltages. Dependence on Cathode Catalyst Layer Composition and on Voltage Conditioning,” *Electrochimica Acta*, Vol. 47, Nos. 22–23, 2002, pp. 3799–3806. https://doi.org/10.1016/S0013-4686(02)00350-X

[17] Zhang, X., Guo, L., and Liu, H., “Recovery Mechanisms in Proton Exchange Membrane Fuel Cells after Accelerated Stress Tests,” *Journal of Power Sources*, Vol. 296, 2015, pp. 327–334. https://doi.org/10.1016/j.jpowsour.2015.07.063

[18] Jomori, S., Komatsubara, K., Nonoyama, N., Kato, M., and Yoshida, T., “An Experimental Study of the Effects of Operational History on Activity Changes in a PEMFC,” *Journal of The Electrochemical Society*, Vol. 160, No. 9, 2013, pp. F1067–F1073. https://doi.org/10.1149/2.103309jes

[19] Yang, S., Choi, S., Kim, Y., Yoon, J., Im, S., and Choo, H., “Improvement of Fuel Cell Durability Performance by Avoiding High Voltage,” *International Journal of Automotive Technology*, Vol. 20, No. 6, 2019, pp. 1113–1121. https://doi.org/10.1007/s12239-019-0104-x

[20] Xing, L., Hossain, M. A., Tian, M., Beauchemin, D., Adjemian, K. T., and Jerkiewicz, G., “Platinum Electro-Dissolution in Acidic Media upon Potential Cycling,” *Electrocatalysis*, Vol. 5, No. 1, 2014, pp. 96–112. https://doi.org/10.1007/s12678-013-0167-9

[21] Ren, P., Pei, P., Li, Y., Wu, Z., Chen, D., and Huang, S., “Degradation Mechanisms of Proton Exchange Membrane Fuel Cell under Typical Automotive Operating Conditions,” *Progress in Energy and Combustion Science*, Vol. 80, 2020, p. 100859. https://doi.org/10.1016/j.pecs.2020.100859

[22] Zago, M., Baricci, A., Bisello, A., Jahnke, T., Yu, H., Maric, R., Zelenay, P., and Casalegno, A., “Experimental Analysis of Recoverable Performance Loss Induced by Platinum Oxide Formation at the Polymer Electrolyte Membrane Fuel Cell Cathode,” *Journal of Power Sources*, Vol. 455, 2020, p. 227990. https://doi.org/10.1016/j.jpowsour.2020.227990

[24] Tsotridis, G., Pilenga, A., De Marco, G., and Malkow, T., “EU Harmonised Test Protocols for PEMFC MEA Testing in Single Cell Configuration for Automotive Applications,” Publications Office of the European Union, Luxembourg, 2015. https://doi.org/10.2790/54653

[25] Zhang, Q., Schulze, M., Gazdzicki, P., and Friedrich, K. A., "Comparison of Different Performance Recovery Procedures for Polymer Electrolyte Membrane Fuel Cells," *Applied Energy*, Vol. 302, 2021, p. 117490. https://doi.org/10.1016/j.apenergy.2021.117490

[26] Sugawara, S., Maruyama, T., Nagahara, Y., Kocha, S. S., Shinohra, K., Tsujita, K., Mitsushima, S., and Ota, K., "Performance Decay of Proton-Exchange Membrane Fuel Cells under Open Circuit Conditions Induced by Membrane Decomposition," *Journal of Power Sources*, Vol. 187, No. 2, 2009, pp. 324–331. https://doi.org/10.1016/j.jpowsour.2008.11.021

[27] Inaba, M., Yamada, H., Umebayashi, R., Sugishita, M., and Tasaka, A., "Membrane Degradation in Polymer Electrolyte Fuel Cells under Low Humidification Conditions," *Electrochemistry*, Vol. 75, No. 2, 2007, pp. 207–212. https://doi.org/10.5796/electrochemistry.75.207

[28] Gazdzick, P., Mitzel, J., Garcia Sanchez, D., Schulze, M., and Friedrich, K. A., "Evaluation of Reversible and Irreversible Degradation Rates of Polymer Electrolyte Membrane Fuel Cells Tested in Automotive Conditions," *Journal of Power Sources*, Vol. 327, 2016, pp. 86–95. https://doi.org/10.1016/j.jpowsour.2016.07.049

[29] Zhang, J., and Datta, R., "Online Monitoring of Anode Outlet CO Concentration in PEM Fuel Cells," *Electrochemical and Solid-State Letters*, Vol. 6, No. 1, 2003, p. A5. https://doi.org/10.1149/1.1523690

[30] Arena, F., Mitzel, J., and Hempelmann, R., "Permeability and Diffusivity Measurements on Polymer Electrolyte Membranes," *Fuel Cells*, Vol. 13, No. 1, 2013, pp. 58–64. https://doi.org/10.1002/fuce.201200116

[31] Pivac, I., and Barbir, F., "Impact of Shutdown Procedures on Recovery Phenomena of Proton Exchange Membrane Fuel Cells," *Fuel Cells*, Vol. 20, No. 2, 2020, pp. 185–195. https://doi.org/10.1002/fuce.201900174

[32] Sugawara, S., Maruyama, T., Nagahara, Y., Kocha, S. S., Shinohra, K., Tsujita, K., Mitsushima, S., and Ota, K., "Performance Decay of Proton-Exchange Membrane Fuel Cells under Open Circuit Conditions Induced by Membrane Decomposition," *Journal of Power Sources*, Vol. 187, No. 2, 2009, pp. 324–331. https://doi.org/10.1016/j.jpowsour.2008.11.021

[33] Inaba, M., Yamada, H., Umebayashi, R., Sugishita, M., and Tasaka, A., "Membrane Degradation in Polymer Electrolyte Fuel Cells under Low Humidification Conditions," *Electrochemistry*, Vol. 75, No. 2, 2007, pp. 207–212. https://doi.org/10.5796/electrochemistry.75.207

[34] Du, F., Dao, T. A., Peitl, P. V. J., Bauer, A., Preuss, K., Bonastre, A. M., Sharman, J., Spikes, G., Perchthaler, M., Schmidt, T. J., and Orfanidi, A., "Effects of PEMFC Operational History under Dry/Wet Conditions on Additional Voltage Losses Due to Ionomer Migration," *Journal of The Electrochemical Society*, Vol. 167, No. 14, 2020, p. 144513. https://doi.org/10.1149/1945-7111/abc83f

[35] Kreitmeier, S., Michiardi, M., Wokaun, A., and Büchi, F. N., "Factors Determining the Gas Crossover through Pinholes in Polymer Electrolyte Fuel Cell Membranes," *Electrochimica Acta*, Vol. 80, 2012, pp. 240–247. https://doi.org/10.1016/j.electacta.2012.07.013

[36] Qi, Z., Tang, H., Guo, Q., and Du, B., "Investigation on 'Saw-Tooth' Behavior of PEM Fuel Cell Performance during Shutdown and Restart Cycles," *Journal of Power Sources*, Vol. 161, No. 2, 2006, pp. 864–871. https://doi.org/10.1016/j.jpowsour.2006.04.137

[37] Zhai, S., Zhou, S., Sun, P., Chen, F., and Niu, J., "Modeling Study of Anode Water Flooding and Gas Purge for PEMFCs," *Journal of Fuel Cell Science and Technology*, Vol. 9, No. 3, 2012, p. 031007. https://doi.org/10.1115/1.4006053